Atomic-structure investigations of neutral einsteinium by laser resonance ionization

Felix Weber,[1,*] Thomas E. Albrecht-Schönzart,[2] Michael Block,[1,3,4] Premaditya Chhetri,[3,4] Christoph E. Düllmann,[1,3,4] Julie G. Ezold,[5] Vadim Gadelshin,[1] Alyssa N. Gaiser,[2] Francesca Giacoppo,[3,4] Reinhard Heinke,[1] Tom Kieck,[1,3,4] Nina Kneip,[1] Mustapha Laatiaoui,[1,3,4] Christoph Mokry,[1,4] Steven Nothhelfer,[1,3,4] Sebastian Raeder,[3,4] Jörg Runke,[3] Fabian Schneider,[1,4] Joseph M. Sperling,[2] Dominik Studer,[1] Petra Thörle-Pospiech,[1,4] Norbert Trautmann,[1] and Klaus Wendt[1]

[1]*Johannes Gutenberg-Universität Mainz, 55099 Mainz, Germany*
[2]*Florida State University, Tallahassee, Florida 32300-32399, USA*
[3]*GSI Helmholtzzentrum für Schwerionenforschung GmbH, 64291 Darmstadt, Germany*
[4]*Helmholtz-Institut Mainz, 55099 Mainz, Germany*
[5]*Oak Ridge National Laboratory, 37831 Oak Ridge, Tennessee, USA*

(Received 4 April 2022; revised 4 July 2022; accepted 29 July 2022; published 21 October 2022)

Excited atomic states of neutral einsteinium were investigated by resonant laser ionization using 10 pg (2×10^{10} atoms) of ^{254}Es. Ten transitions from the $5f^{11}7s^2\,{}^4I^o_{15/2}$ ground state to even-parity states were investigated in detail, via studies of lifetimes and further excitation steps into higher-lying odd-parity states below and above the first ionization potential. This led to the identification of 37 previously unknown odd-parity energy levels in the region between 37 000 and 42 500 cm^{-1} and a number of autoionizing states, which ensure a high ion yield in resonant ionization. Rydberg states were identified and the corresponding Rydberg series converging either to the ionic ground or an excited state were analyzed to determine the first ionization potential of einsteinium to a value of $E_{\mathrm{IP}} = 51\,364.58(14)_{\mathrm{stat}}(50)_{\mathrm{sys}}\,\mathrm{cm}^{-1}$, improving the previous result by a factor of four.

DOI: 10.1103/PhysRevResearch.4.043053

I. INTRODUCTION

Fundamental atomic properties of the heavy actinides are generally not well known as investigations of their atomic structure are limited by the scarce availability of these elements. To validate theoretical predictions on these highly correlated systems and to provide more data on the atomic properties along the entire periodic table of elements up to the superheavy elements with atomic number $Z \geqslant 104$, comprehensive experimental investigations on heavy actinide elements are desirable [1]. The atomic spectra are highly complex, and they are strongly influenced by relativistic effects, electron correlations, and quantum electrodynamics. As $Z\alpha \approx 1$ and the fine structure is no longer a small correction, perturbative treatments are not applicable. Instead, state-of-the-art fully relativistic many-body methods have to be utilized for theoretical calculations of atomic spectra. Also, the finite size of the nucleus, predicted to have even a nonuniform charge distribution, add another layer of complexity to such calculations.

Albeit elements up to fermium (Fm, $Z = 100$) can be produced in weighable quantities since the 1960s in high neutron flux nuclear reactors, such as the high flux isotope reactor (HFIR) at the Oak Ridge National Laboratory (ORNL) [2], their atomic structure remains scarcely known. Elements above fermium can only be produced in single-atom amounts in accelerator-based on-line experiments. Laser spectroscopy experiments to study the atomic structure of such elements have so far only been performed on nobelium (No, $Z = 102$) [3–5].

The element einsteinium (Es, $Z = 99$) was discovered together with fermium in 1952 in material retrieved from a thermonuclear explosion test site [6]. One year later, einsteinium was purposely produced artificially by neutron irradiation of plutonium in a reactor and by nuclear fusion reactions of nitrogen ions with uranium nuclei, allowing for the determination of first nuclear properties [7–11]. Nearly all spectroscopic information on the atomic structure of einsteinium comes from measurements of emission spectra using electrodeless lamps [12–14]. These experiments were carried out with total amounts of up to 100 µg ^{253}Es ($T_{1/2} = 20.47$ d) using reactor-bred material. Additional energy levels were later derived by reanalyzing the data, but only slow advances were achieved as the infrared region of the einsteinium spectrum was not covered [15]. Further studies were hampered by the unavailability of larger quantities of einsteinium. In 1998, first laser spectroscopic studies, using the resonance-ionization spectroscopy (RIS) method [16,17], were carried out on ^{254}Es. The first ionization potential (IP) was determined to $E_{\mathrm{IP}} = 51\,358(5)$ cm^{-1} (2σ uncertainty) by measuring ionization thresholds in varying external electric fields [18,19]. This technique often suffers from a reduced precision compared to the analysis of Rydberg convergences, but nevertheless is frequently used in open *f*-shell elements, as the

*wfelix02@uni-mainz.de

complexity of their spectra commonly prevents a conclusive assignment of individual resonances to a specific Rydberg series [20]. Due to the limited availability and the rapid nuclear decay of einsteinium, no further measurements on the atomic structure in einsteinium have been carried out to date. Thus, the knowledge on the overall atomic structure including level energies and configurations, remains scarce, with just about 40 atomic levels reported in literature [15,21]. For some of these levels also the hyperfine structure parameters have been extracted, with highest precision for the ground state [22].

RIS, based on efficient ionization schemes, offers inherent elemental selectivity, rendering the technique useful for element separation, e.g., at on-line ion beam facilities such as CERN-ISOLDE [23]. In this paper, we present detailed studies on level positions and excitation schemes in einsteinium involving numerous atomic levels, both lower-lying as well as around the IP, carried out at the off-line RISIKO mass separator facility of Johannes Gutenberg University Mainz (JGU) [24]. The investigations became possible by the availability of pg samples of ^{254}Es ($T_{1/2} = 275.7$ d), and benefited from recent advances regarding sensitivity and selectivity of in-source RIS applied in combination with high transmission mass separation. These include an automated long-term control of the laser frequencies as well as technical optimizations in the laser ion source unit, preventing cold spots. A rather similar experimental approach was used, e.g., for laser spectroscopic studies on so far missing low-lying levels in neutral actinium [25]. The identification of two-step ionization schemes for einsteinium via strong autoionizing states (AIS) was achieved for ten different first excited states (FES). For all of these FES, the lifetime or at least an upper limit for it was determined. Additionally, high-lying atomic odd-parity levels were measured applying three-step ionization schemes. Results are compared with the known transitions and energy levels reported in Refs. [14,15]. The obtained AIS spectra were used to determine the first IP as an important fundamental property of einsteinium, which specifies its chemical behavior. For this purpose, Rydberg series converging towards either the IP or to a low-lying excited level in the Es^+ ion were analyzed. A detailed analysis of the hyperfine structures and the isotope shifts observed in several of the ground-state transitions investigated here was already published recently [26].

II. EXPERIMENTAL SETUP

The einsteinium sample was produced in the HFIR at ORNL using targets containing 6.3 g of curium (^{244}Cm to ^{248}Cm). By successive neutron captures followed by β^- decays, the curium isotopes transmuted to berkelium, californium, and finally to einsteinium and fermium isotopes. After 90 days of cooling to eliminate unwanted short-lived nuclides coproduced within the targets, the einsteinium was chemically separated at the ORNL's Radiochemical Engineering Development Center [27]. A sample containing about 2 ng of ^{253}Es, 4 ng of ^{254}Es, and 4 pg ^{255}Es was shipped to the Institute of Nuclear Chemistry at JGU, where it was dissolved in 0.1 M nitric acid. From this solution three aliquots, each containing among others about 10^{10} atoms of ^{254}Es (≈4.2 pg), were pipetted onto small pieces of zirconium foil, dried and folded for complete enclosure and to fit into the mass separator ion source. All measurements presented here were carried out on ^{254}Es.

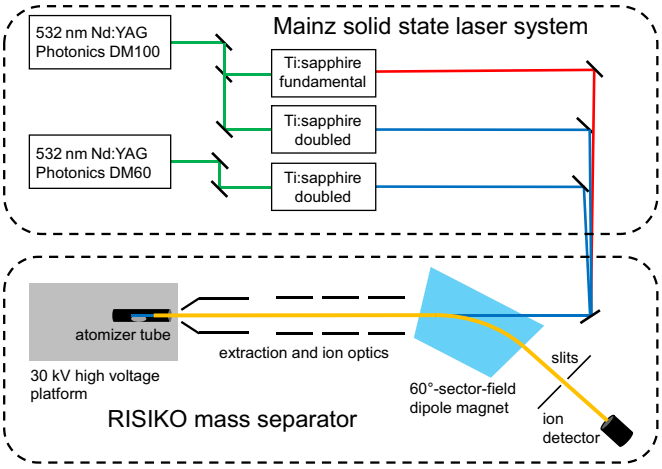

FIG. 1. Sketch of the RISIKO mass separator and the solid-state laser system. More details are given in the text and in Ref. [24].

The RIS measurements were conducted at the RISIKO mass separator facility at the Institute of Physics at JGU. The setup is described in its standard configuration in detail in Ref. [24]. The wrapped sample was directly inserted into the tantalum atomizer tube (length: 35 mm, inner diameter: 2.5 mm) of the ion source, which can be heated resistively to a temperature of about 2000 °C, omitting the usual sample reservoir. This simplified arrangement suppresses unspecific background when the cavity is carefully operated and gently heated to the lowest suitable temperature for einsteinium evaporation. A sketch of the RISIKO setup including the solid state laser system used for resonant ionization is depicted in Fig. 1. At about 900 °C the neutral einsteinium atoms evaporate and become available for subsequent ionization by the laser radiation. The singly charged ions were extracted from the ion source, accelerated by a 30 kV static electric potential, and afterwards guided through a 60° − sector − field dipole magnet for separation according to their mass-to-charge ratio. Distant and neighboring masses in the ion beam are suppressed with a typical mass resolving power of $M/\Delta M \approx 600$. After passing the separation slit, the mass-separated ions were counted by a secondary electron multiplier (MasCom MC-217).

The solid-state laser system consists of two commercial frequency-doubled Nd:YAG lasers operating at 532 nm with 10 kHz repetition rate, which are used to pump up to three custom-built Ti:sapphire lasers. Each of those is pumped with up to 18 W and can be tuned between 700–1000 nm in fundamental and 350–500 nm in a frequency doubled operation mode using a resonator-internal beta barium borate (BBO) crystal. A more detailed description of a similar laser system used at the ISOLDE-RILIS is given in Ref. [28]. All wavelengths are measured with a wavelength meter (High Finesse WSU-30) via fiber-switches with a quoted 3σ precision of 20% of the laser linewidth. The wavelength meter is regularly calibrated during the measurement with a Rb-saturated absorption locked external cavity diode laser to ensure the specified accuracy. The tunable lasers feature au-

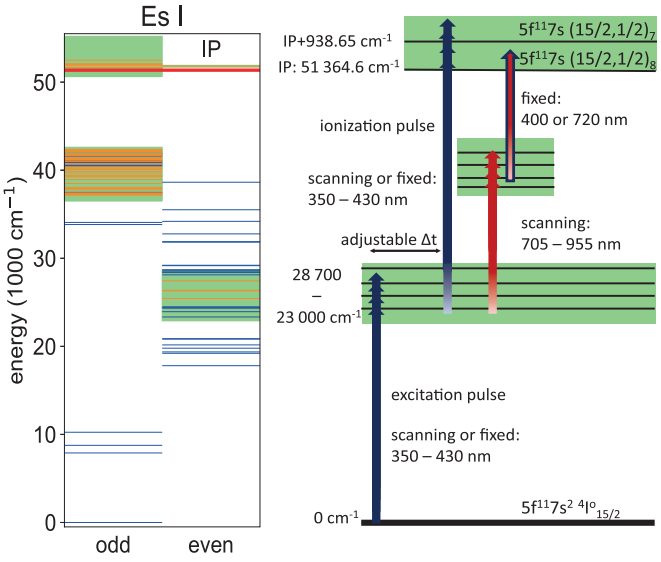

FIG. 2. Left: Es I level scheme: Blue lines indicate all previously known energy levels from [15,21], green-shaded regions were studied in this paper with newly identified levels indicated by orange lines. Around the IP (red line), only the strongest AIS as given in Table I are indicated. Right: Sketch of the different ionization schemes studied in this paper. Detailed information on the individual excitation schemes is given in Table I.

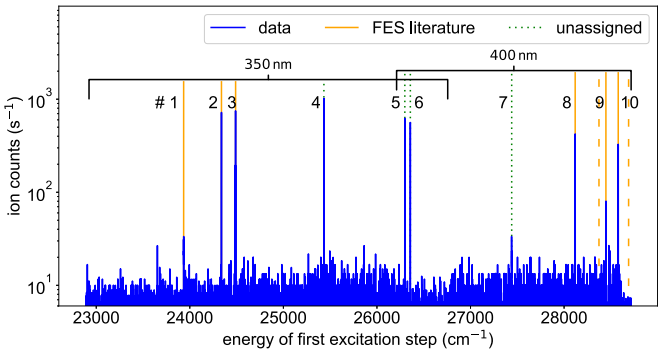

FIG. 3. Wavelength scan on ground-state transitions in Es I showing ten FES resonances. The ionization laser was operated at fixed frequency, $\lambda_2 = 400$ nm and $\lambda_2 = 350$ nm for the high- and low-energy region in this scan, respectively, as indicated in the spectrum. The solid-orange lines represent known FES with assigned configurations from literature [15,21]. The dashed-orange lines are also listed there, but were not seen in this scan. The dotted green lines represent known transitions from literature, which could previously not be assigned to energy levels.

tomatic frequency scanning in the fundamental as well as tracked intracavity phase matching for the second harmonic generation (SHG) [29]. The power is up to 1.8 W for fundamental wavelength and 800 mW for the SHG output with a laser pulse length between 30 and 50 ns. The linewidth of the broadband scanning laser lies within the range of 5 to 7 GHz (0.17 to 0.23 cm^{-1}). However, all wavelength measurements were done in the fundamental laser light before SHG. A laser linewidth of 4.5 GHz in the fundamental beam leads to a systematic uncertainty of 0.01 cm^{-1} (1σ) and accordingly to 0.02 cm^{-1} for frequency doubled light. A master clock (Quantum Composer 9530) triggers the pump lasers and is used to control a variable time delay between the laser pulses of the two pump lasers. This is used to guarantee temporal overlap of laser pulses during the frequency scans and allows measuring the lifetimes of excited energy levels by delaying one of the pulses by precisely defined time intervals.

III. LASER SPECTROSCOPIC RESULTS

All energy levels of neutral einsteinium (Es I) known prior to our study are shown as blue lines in Fig. 2 (left), separately for odd- and even-parity states. The graph highlights the regions investigated within this paper by green boxes. Fifty-one energy levels newly identified in this paper are indicated by orange lines. To access these regions, the different two- or three-step ionization schemes were applied, as depicted in Fig. 2 (right). As FES, ten different levels in the range of 23 000 to 28 700 cm^{-1} were studied in the following way:

(i) the energetic positions were determined

(ii) odd-parity AIS were identified in a two-step ionization scheme

(iii) odd-parity second excited states were searched in a three-step ionization scheme using a fixed-frequency laser for the third excitation step

(iv) the lifetime of the FES was measured

(v) odd-parity Rydberg levels were identified in the spectrum around the IP.

All energy levels given in this paper refer to the centroid of the measured resonance peaks, which partly exhibit rather broad unresolved hyperfine structure splittings in the order of up to 100 GHz (3.3 cm^{-1}) [26]. A maximum scanning speed of approximately 20 cm^{-1}/min was used in all wide-range laser scans and 10 data points were recorded per wavenumber.

A. First excited states

Initially, ground-state transitions were searched for by scanning one laser in the range from 350 to 430 nm, while keeping the ionization laser with a power of 300 mW at a fixed wavelength of either 350 nm (for scanning the excitation laser between 22 800 and 26 800 cm^{-1}) or 400 nm (for scanning the excitation laser between 26 250 and 28 600 cm^{-1}). Thereby the overlapping area of the wavenumbers was scanned twice. The average power of the scanning laser was between 50 mW and 300 mW determined essentially by the gain profile of the Ti:sapphire laser medium. The recorded spectrum is shown in Fig. 3.

Ten resonances were identified, with solid-orange lines representing known energy levels from literature [14,15]. Two dashed orange lines above 28 000 cm^{-1} represent expected transitions to reported levels, which were not seen in this scan. From these two, the lower state at $E_1 = 28\,372.78$ cm^{-1} became just detectable with strongly extended accumulation times, but was not used in further measurements due to the weak signal. The four dotted-green lines represent transitions, which were reported from the optical-spectrum analysis in [14], but were not matched to an energy level. In the compilation of actinide spectra [21], the spectral lines No. 1, 4, and 5

TABLE I. Overview of studied ionization schemes and the observed FWHM of the FES during the frequency scan as a hint for the hyperfine structure width of the corresponding transition. The configurations and angular momenta are taken from [15,21,26]. It should be noted that the literature values refer to ^{253}Es [14,15,21], whereas the values determined in this paper are obtained for ^{254}Es. The FES lifetime was measured by temporally delaying the ionization pulse with respect to the excitation pulse (see Sec. III D). For all FES, we provide the AIS position resulting in the highest signal in the spectrum. The AIS enhancement is given as a rough estimate of the ratio of ion signal with the second laser tuned to the resonance to that obtained by nonresonant ionization. In addition to the statistical uncertainties given here, a systematic uncertainty of 0.02 cm^{-1} has to be added for the AIS. The uncertainties are discussed in the text.

No.	$E_{1,254}$ (cm^{-1})	$E_{\mathrm{lit},253}$ (cm^{-1})	FWHM (cm^{-1})	Configuration	τ (ns)	AIS (cm^{-1})	Signal on AIS (s^{-1})	AIS enhancement
1	23 934.20(5)[a]	23 934.19	2.6	[b]$7s7p\,(^3P_2)\ 17/2$	1133(51)	52 049.70(26)	400	20
2	24 338.23(5)[a]	24 338.29	1.1	[b]$7s\,7\,p\,(^3P_2)\ 15/2$	484(11)	51 442.45(26)	3500	50
3	24 489.12(5)[a]	24 489.42	1.1	[b]$7s\,7\,p\,(^3P_2)\ 13/2$	380(6)	51 445.85(26)	2800	200
4	25 433.26(14)	25 433.12	1.0		124(8)	51 979.02(29)	8000	600
5	26 297.92(20)	26 297.98	0.6		35(3)	51 663.53(32)	4000	25
6	26 357.00(20)	26 356.96	0.7		$\lesssim$30	51 930.18(32)	6200	25
7	27 440.06(5)[a]	27 440.10	3.0	$13/2$	443(19)	51 677.37(26)	230	20
8	28 118.49(20)	28 118.58	0.7	[b]$7s7p\,(^1P_1)\ 13/2$	$\lesssim$30	52 488.81(32)	3800	75
9	28 446.86(5)[a]	28 447.02	2.9	$5f^{11}\,7s7p\ 13/2$	$\lesssim$30	52 004.01(26)	13500	270
10	28 578.49(20)	28 578.71	1.6	[b]$7s7p\,(^1P_1)\ 17/2$	$\lesssim$30	52 049.12(32)	900	100

[a]Determined in [26].
[b]Means $5f^{11}\ (^4I_{15/2})$.

(cf. Table I and Fig. 3) were incorrectly assigned to transitions between excited states, while in the more recent publication [15] the energetic position of No. 1 is treated to represent an energy level and thus the spectral line is correctly ascribed to a ground-state transition. All resonances observed in our scan can be safely assigned to ground-state transitions, as no low-lying state in einsteinium is substantially thermally populated in the ion source. A further confirmation of the assignment arises from the investigations on high-lying odd-parity levels, which were addressed from different FES. Although the spectral lines have been observed before, RIS enables a much more profound assignment of energy levels compared to the analysis of emission spectra. The measured FES are summarized in Table I, where the FWHM refers to the linewidth observed during the scan. All resonances were individually scanned a second time with a reduced laser linewidth in the order of 1.5 to 2.5 GHz (0.05 to 0.08 cm^{-1}) to precisely determine their energetic position. This reduced laser linewidth ($\approx$2 GHz in the fundamental) results in a systematic uncertainty of the determined level energy of $\approx$0.01 cm^{-1} for all FES. A comparison between the fast laser scans with lower resolution and the slower scans with increased resolution is depicted in Fig. 10 in the Appendix. The center of gravity determined by fitting Gaussian curves to the broadband data differs for these 10 measured resonances in all cases by less than 0.25 cm^{-1} from the data obtained with higher resolution. Hence, the statistical uncertainty of all wide range broadband laser scans is conservatively set to 0.25 cm^{-1}. An overall precision of 0.05 cm^{-1} is achieved in the narrowband scans for FES No. 1,2,3,7, and 9, where the hyperfine structure is resolved and an analysis was performed in Ref. [26]. For the other five transitions, the hyperfine structure is not resolved sufficiently well to perform an independent hyperfine structure fit. However, the hyperfine structure parameters of the ground state are known and support a restricted analysis, while the fit uncertainty is possibly underestimated due to a shift of the centroid, caused by improper intensities of individual hyperfine structure components. Conservatively, an uncertainty of 50% of the FWHM, determined in the higher resolution scans, was taken for these unresolved structures (FES No. 4,5,6, and 8). In case of FES No. 10 the hyperfine splitting is just partly resolved. However, the intensities of the hyperfine structure components deviate from calculated ones and the precision of the centroid as for the case of unresolved structures, is set to 0.2 cm^{-1}. Systematic uncertainties for the FES are already included in the specified precision.

The energetic positions determined for ^{254}Es in this paper is compared with the literature values for ^{253}Es, given in the second column of Table I [14,15,21]. For all excited levels with a configuration assigned in literature, the magnitudes of the isotope shifts and the signs agree with the expectation for a $5f^{11}7s^2$ to $5f^{11}7s7p$ transition. Due to the ground state with $J_{\mathrm{GS}} = 15/2$ the excited energy levels accessible via laser spectroscopy are limited to $J_{\mathrm{FES}} = 13/2$, $15/2$, or $17/2$. In addition, only reasonably strong transitions can be observed which generate ion signals above the background level. Aside of excluding the detection of weakly populated excited levels, also levels exhibiting a weak ionization step, are not seen. One of these two points might explain the nondetection of the level at 28 689.6 cm^{-1} given in Ref. [14].

B. Odd-parity AI states

In a next measuring series, the ionization laser was scanned around the IP for all ten FES, giving access to the odd-parity spectrum from 50 640 to 54 330 cm^{-1}. Figure 4 shows the relevant part of the frequency scans exhibiting numerous broad continuum structures and a high density of AIS. The level density in the region below the first excited state of the einsteinium ion (Es II) located at $\mathrm{E_{IP}} + 938.65$ cm^{-1} [21] is particularly high. A closer look reveals weak Rydberg series converging to this state in at least seven of the spec-

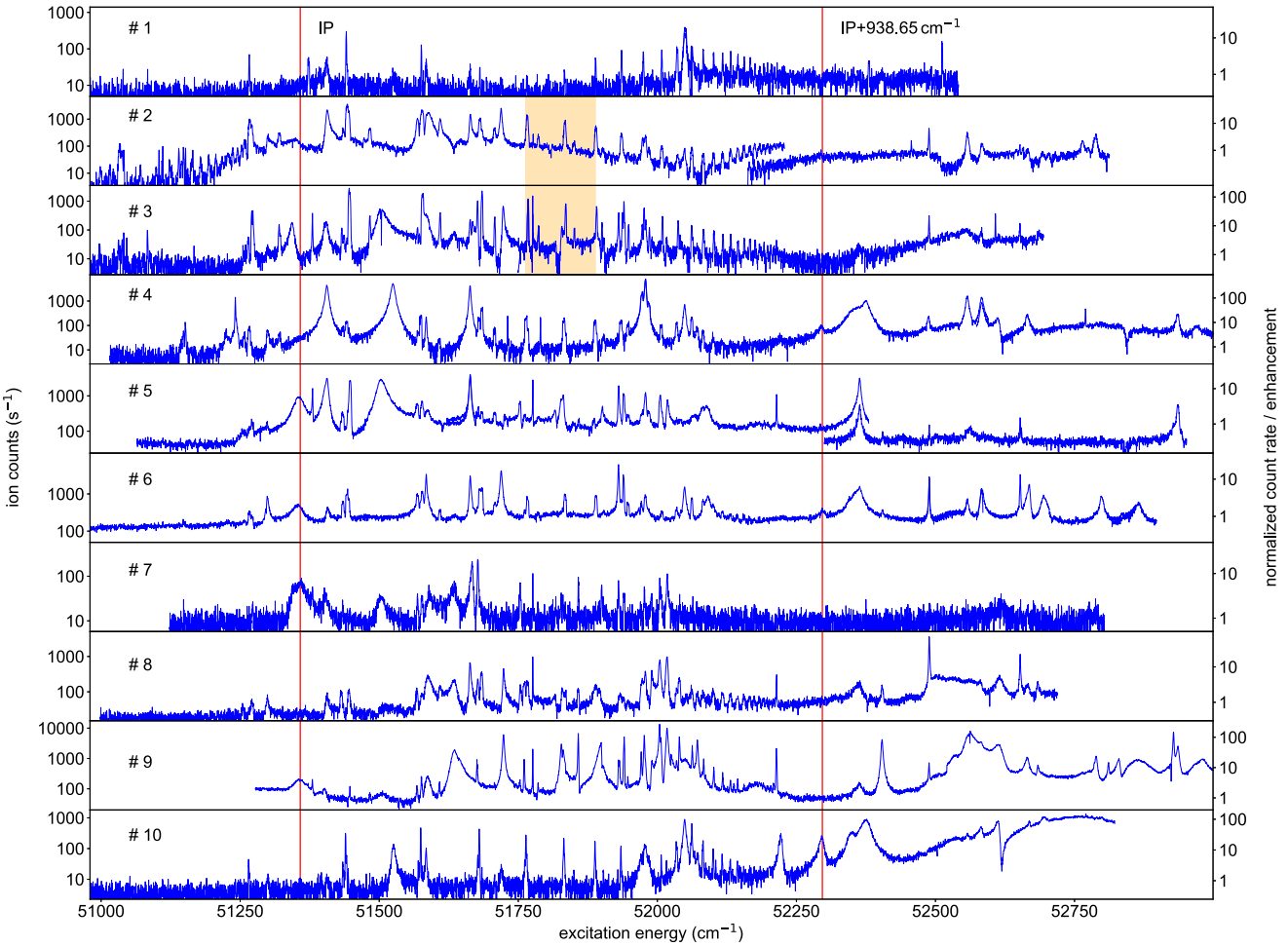

FIG. 4. Spectra showing odd-parity states of einsteinium obtained in a two-step ionization scheme by scanning the second step around the IP for the ten different FES No. 1 to No. 10 as indicated and specified in Table I. On the left *y* axis the count rate during the laser scans is shown. On the right *y* axis an enhancement factor is given by normalizing the count rates to their individual baseline of nonresonant ionization. All spectra show a specifically high density of resonances in the region between the IP and the first excited state of the Es^+ ion, ascribed to a large extend to converging Rydberg series. The highlighted regions are shown in more detail in Fig. 8.

tra. These series are evaluated in Sec. III E. The resonances with the highest ion yield are suitable for high-resolution laser spectroscopy and were used for the hyperfine structure measurements mentioned above [26]. A comparison of the most efficient ionization schemes for the ten identified FES is given in Table I. The AIS indicate the energy position at which the largest ion signal was observed and not necessarily the centroid of the corresponding resonance structure. The statistical uncertainty is composed by 0.25 cm^{-1} due to the fast scanning of the second laser, as discussed before, and additionally the uncertainty in the FES. Here it should be noted that the excitation laser for FES No. 1 was set to 23 933.4 cm^{-1} during the laser scans and thus the AIS energy is calculated using this value. Systematic uncertainties due to the wavelength measurement are 0.02 cm^{-1}. Due to varying ion source conditions during the different scans, we specify both, the measured counting rate with the second laser tuned to the AI resonance as well as a second-step-enhancement factor. The latter is defined as the ratio between the ion signal with the second laser tuned on the AI resonance and the nonresonant ionization to the continuum. This nonresonant ionization rate was used as normalization factor and can be extracted from Table I by dividing the signal on AIS by the AIS enhancement.

C. Three-step ionization

Applying a three-step ionization scheme allows for the search for odd-parity energy levels in the region between 36 500 and 42 500 cm^{-1}. For this purpose each ground-state transition from Table I was resonantly excited consecutively while scanning the fundamental output wavelength of a second Ti:sapphire laser and recording respective scans via the intensity of the ion signals. The first excitation steps were tuned to their centroids as given in Table I for all scans, except for the one at 23 934.2 cm^{-1}, where the laser was set to 23 933.4 cm^{-1} for maximum signal intensity. Correspondingly, this value was taken to calculate the respective energies of the upper states. When the scanning laser was resonant to a transition, a third laser, either in fundamental or SHG mode was used for nonresonant ionization (cf. Fig. 2). Figure 5 shows the spectrum with the signals from the higher-lying

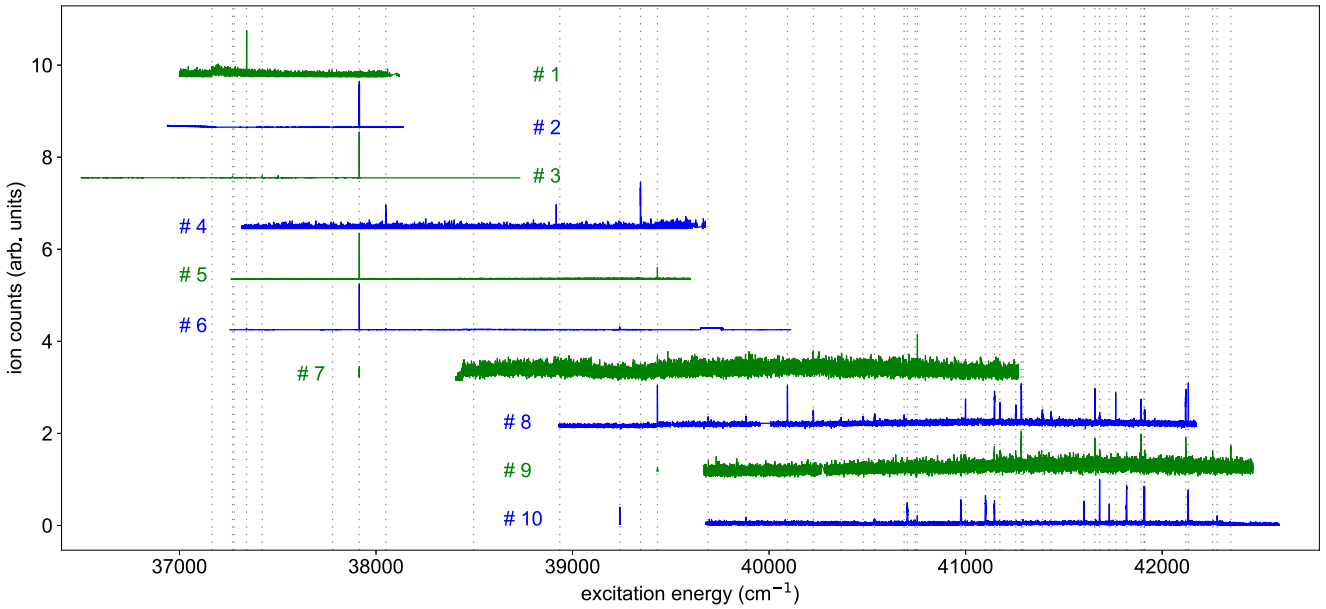

FIG. 5. Scan for higher-lying odd-parity second excited states in a three-step excitation scheme in Es I starting from different FES with their energies added to the scanning laser wavenumber. The dotted lines indicate where energy levels were assigned. The intensities in all scans are normalized to one and an arbitrary offset for each trace is added for distinction. About half of the excited levels were measured starting from at least two different FES. In many spectra, the second excited state at 37 915 cm^{-1} shows a particularly high count rate, as the ionization laser accidentally hits an AIS.

second excited states. Half of these states can be addressed starting from more than one FES. All observed energy levels are summarized in Table II together with the information in which excitation scheme they were observed. The energy positions of second excited states are determined as follows: According to Fig. 10 the transition to FES No. 4,5,6, and 8 is relatively narrow, so that the excitation laser populates all hyperfine structure levels. Thus, the second excitation step also addresses the complete hyperfine structure and an accurate energy position of the second excited state can be determined. For all other first steps, an individual distribution of hyperfine structure components is possibly selected so that a precise information about the centroid of the second excitation step is not available. Therefore, the energy obtained from the narrow FES is always given as the center whenever transitions from different FES to the same state are available. The situation here is similar to that described in Sec. III A, so that the uncertainty due to the unresolved hyperfine structure and the fast scan is 0.25 cm^{-1}. In addition, the uncertainty from the first step must be taken into account. If a state has been excited by several narrow FES, the mean value is given. Sixteen states are observed exclusively from broad FES, resulting in a population of a limited subset of hyperfine structure components. Thus, the uncertainty has to be determined differently. For 21 states, the deviation of energy positions obtained from broad FES and those obtained from narrow FES can be compared. From the distribution of deviations for a total of 31 values (some of the 21 states were seen starting from more than one broad FES), the uncertainty can be determined to be 0.54 cm^{-1}. In addition, the uncertainty from the first step must also be considered for the 16 states, which were excited from broad FES. All statistical uncertainties are given in Table II. Systematic uncertainties of 0.01 cm^{-1} arise from the wavelength measurement and are small compared to the statistical ones. Eleven previously known energy levels from [15] are provided in Table II for comparison, while the remaining 37 levels are reported here for the first time. Considering the uncertainties determined in this paper and an unknown isotopic shift, both values are in good agreement. With the exception of the level at 37 485.58 cm^{-1}, all levels reported in Ref. [15] that lie within the scanning range and can be populated by dipole transitions were detected, demonstrating the high sensitivity of our measurements. The angular momenta of eight states were determined to be $J = 15/2$ because they were accessible from different FES having J_{FES}=13/2 and J_{FES}=17/2 (see Table II).

Most of the levels were observed in a nonresonant ionization scheme resulting in a weak signal. In many of the spectra, the line at an excitation energy of $E_2 = 37\,915.0$ cm^{-1} showed particularly high intensities because the ionization laser was coincidentally populating an AIS. Its energy is determined to be $E_{\mathrm{AIS}} = 51\,823.4$ cm^{-1}. As given in Table II, the second excited state at $E_2 = 37\,915.0$ cm^{-1} can be reached from five different FES. Thus, in total five fully resonant and strong three-step ionization schemes can be assigned, using the same second excited state and the same AIS. In the future, these three-step ionization schemes could be very useful for specific experiments, as they provide higher elemental selectivity compared to a two-step scheme, for which usually high-power UV radiation is required that could lead to undesired nonresonantly ionized background.

D. Lifetimes of excited states

The lifetime is a fundamental property of an atomic state, which is directly related to the transition strengths of possible

TABLE II. Measured odd-parity energy levels in ^{254}Es. The literature value and angular momentum is given for 11 previously known energy levels in ^{253}Es [15]. Additionally, the FES from which the transition was observed (cf. Table I) is given and if possible J is specified or limited to two possible values. In addition to the statistical uncertainties given here, a systematic uncertainty of 0.01 cm^{-1} has to be added. Both uncertainties are discussed in the text. For the literature values, no uncertainties are specified in the referenced paper.

$E_{2,254}$ (cm^{-1})	$E_{\mathrm{lit},253}$ (cm^{-1})	J	Seen from FES
37 166.07(54)		15/2, 17/2	1,2
37 269.77(54)			3
37 278.66(54)			3
37 341.19(23)		15/2	1,3,5,6
37 421.13(32)			3,5
37 779.06(32)			6
37 914.94(23)		13/2, 15/2	2,3,5,6,7
38 050.08(22)			4,6
38 496.27(32)			6
38 935.09(23)			6,8
39 240.82(32)			6,10
39 346.42(29)			4
39 431.83(23)			5,7,8,9
39 690.15(32)			8
39 882.34(19)		15/2	5,6,8,10
40 093.63(23)			6,8
40 225.21(32)			7,8
40 366.68(32)			8,9
40 478.73(32)	40 478.25	13/2	8
40 537.06(32)	40 536.93	15/2	8,10
40 687.03(32)			8
40 703.62(58)	40 704.55	19/2	10
40 743.65(58)	40 744.46	17/2	10
40 754.31(32)		15/2	7,8,10
40 976.44(58)	40 977.22	19/2	10
40 999.45(32)			7,8,9
41 101.22(58)	41 101.95	17/2	10
41 146.83(32)		15/2	8,9,10
41 174.28(32)			7,8,9
41 255.57(32)			8,9
41 283.28(32)			8,9
41 292.58(58)			10
41 391.29(32)			8
41 435.36(32)			8
41 602.17(58)	41 602.40	17/2	10
41 657.89(32)			8,9
41 681.62(32)	41 682.02	15/2	8,9,10
41 730.73(58)			10
41 763.54(32)			8
41 818.75(58)	41 819.18	19/2	10
41 892.08(32)			8,9
41 907.36(58)	41 907.59	17/2	10
41 910.36(32)	41 910.78	15/2	8,9,10
42 119.94(32)			8,9
42 133.33(32)		15/2	8,10
42 256.79(54)			9
42 280.26(58)			10
42 349.29(54)			9

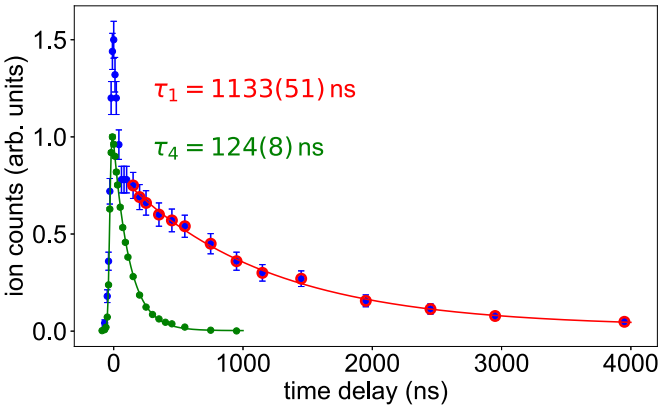

FIG. 6. Determination of the lifetime for two different excited states in a two-step scheme, with the subscript referring to the FES from Table I. The data are given by the blue (FES No. 1) and green (FES No. 4) dots. The subset of the data considered in the fit for FES No. 1 is shown by the red circles. Solid lines represent fits to the data. For details see text.

optical decay channels. As these properties can be predicted by atomic theory, their experimental determination helps with the identification and the assignment of atomic levels. To measure the lifetime, the temporal evolution of the FES population was probed by recording the ion signal as function of the ionization-pulse delay in a two-step ionization scheme. For suitable signal strength, the corresponding AIS was used for ionization for each FES, as given in Table I. The time profile of the laser pulses can be considered with reasonable accuracy as Gaussian. The resulting overall time profile in the measurement can thus be expressed as a convolution of a Gaussian profile with an exponential decay [30]. Lifetimes can be determined with this method to a lower limit of about 30 ns. This is slightly below the laser pulse length. An upper limit of about 3 µs results from deexcitation due to collisions with the oven wall or other atoms inside the hot atomizer cavity of the laser ion source [31]. In some cases, the signal is additionally enhanced when both laser pulses coincide. This is ascribed to the situation that the ionization laser is generating an ionization channel whilst the first excitation laser is still present. The strength of this effect highly correlates with the laser power applied to the first step. In such cases, the lifetime can be extracted by fitting the tail of the decay with an exponential function. Two examples are given in Fig. 6. For FES No. 1 (blue data set) only the exponential decay is fitted to a subset of the data (indicated by red circles) to extract the lifetime, while for FES No. 4 (green data set) all data points are described by the convolution. For the latter, it was verified that the result agrees with the result obtained from fitting an exponential decay to a subset of the data neglecting data points for short delay times. The extracted lifetimes with their uncertainties determined from the fits are included in Table I. Possible systematic uncertainties, e.g., due to a temporal decrease in the ion signal, are not taken into account here as they are considered to be negligible. Saturation can easily be achieved in transitions to short-lived excited states;

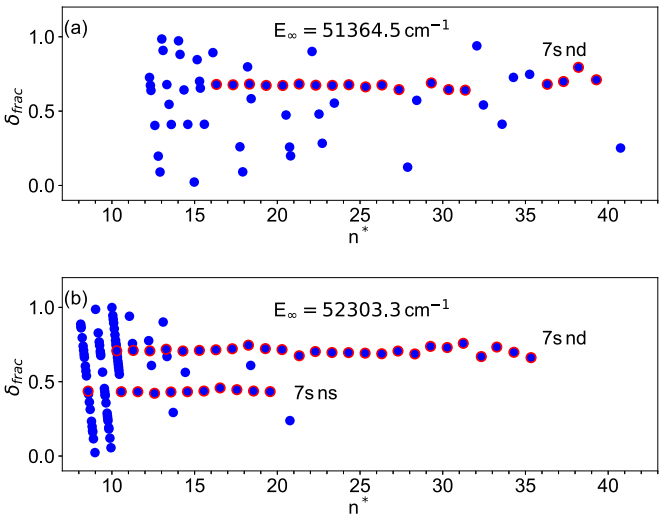

FIG. 7. Fractional part of the quantum defect δ_{frac} as function of the effective principal quantum number n^* for the excitation scheme starting from FES No. 2 at 24 338.2 cm^{-1}. Panel (a) refers to the spectrum below the IP, while panel (b) shows all observed energy levels up to the first excited state in the Es^+ ion (*cf*. Fig. 4 panel No. 2). Assigned Rydberg levels are highlighted in the plot in red. More details on the assignment are provided in the text.

this promotes efficient ionization. On the other hand, atomic states with longer lifetimes can be of relevance in hyperfine structure measurements to increase the resolution by delaying the ionization pulse [32].

E. Ionization potential

In the spectra above the IP, we observed several Rydberg series converging to the lowest excited state in Es II. One series was found below the IP, that converged directly to this limit. Rydberg states were identified by observing a trend in the quantum defect $\delta(n)$, which can be calculated applying the Rydberg-Ritz formula

$$E_n = E_\infty - \frac{R_\mu}{(n-\delta(n))^2} = E_\infty - \frac{R_\mu}{(n^*)^2}, \qquad (1)$$

where E_∞ is the series limit, R_μ the Rydberg constant for finite nuclear mass, and n the principal quantum number. The energy of each Rydberg level was determined by a Gaussian fit. Hyperfine structure is not considered in the IP analysis and we always refer to the center of the measured resonance. The uncertainty is again 0.25 cm^{-1} due to the unresolved hyperfine structure in fast broadband scans. However, this does not necessarily include the uncertainty for the centroid of Rydberg levels, since the first excitation laser might select only a subset of the hyperfine structure components for broad FES. Instead, the uncertainty here should be understood as a statistical uncertainty of the individual resonances within the series. The artificial shift of Rydberg level centroids due to the selective excitation of a certain F ensemble is considered as a systematic error, which finally affects the convergence limit of the series. Figure 7 shows the fractional part of the quantum defect δ_{frac} in dependence of the calculated effective principal quantum number n^* for the observed resonances

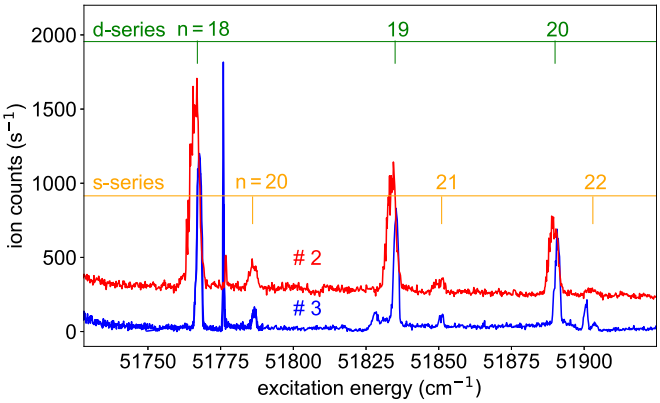

FIG. 8. Magnification of the obtained spectra [cf. Fig. (4) of scheme No. 2 (blue) and 3 (red) with an added offset of 200 counts per second for better visualization. The *d*-series shows a shift between both spectra, which can be explained by different fine structure configurations of the corresponding states.

starting from FES No. 2 at 24 338.2 cm^{-1}. With a properly chosen convergence limit, a Rydberg series shows a rather constant quantum defect for higher n as described in the Ritz expansion [33]

$$\delta(n) \approx \delta_0 + \frac{\delta_1}{(n-\delta_0)^2} + \frac{\delta_2}{(n-\delta_0)^4} + (\cdots). \qquad (2)$$

Minor local fluctuations might arise from level interactions due to configuration mixing. The analysis of trends in $\delta(n)$ enables the unambiguous assignment of many resonances to individual series. Nevertheless, there are some regions in the spectrum where resonances are close together and an assignment just by the quantum defect is not applicable. This is, e.g., the case for low values of n^* in Fig. 7. Many of those resonances are either multielectron excitations or Rydberg series converging to a different series limit. In fact, some of the low-n^* points in Fig. 7(b) were assigned to the Rydberg series converging directly to the IP. In addition, other characteristics such as intensity and width of the resonances were taken into account for a sound assignment. The gap in the mapping between $n^* = 32 - 35$ in Fig. 7(a) is caused by a strong perturbation (cf. Fig. 4 panel No. 2 around $E = 51\,270$ cm^{-1}). Based on the electron configuration of $5f^{11}7s7p$ in the FES, an *s*- or *d*-series is expected. The fractional quantum defect $\delta_{\text{frac}} \approx 0.7$ can therefore be assigned to a *d*-series and an absolute value of $\delta_0 \approx 3.7$ is assumed based on theoretical predictions in Ref. [34]. In the same way, an *s*-series can be assigned to $\delta_{\text{frac}} \approx 0.4$ with an absolute value of $\delta_0 \approx 5.4$. Figure 8 shows the magnification of a part of the spectra from schemes No. 2 and 3, with the assigned Rydberg levels. While the *s*-series is perfectly aligned here, the *d*-series is slightly shifted between both schemes, which means that the corresponding states might not have the same configuration or angular momentum J. This assumption is confirmed by varying values of δ_0 in Table III for these two different FES. Most likely, these are different fine-structure levels, which are populated starting from the individual FES. Such a splitting of a *d*-series into several fine structure levels with different quantum defects is also seen in Rydberg series of holmium,

TABLE III. Overview of the results obtained from Rydberg series fits for the determination of the first IP of ^{254}Es, for seven different FES and altogether nine series. Data include the principal quantum numbers n for the sequence(s) of observed levels, the parameters of the Rydberg-Ritz formula, the convergence limit, the resulting IP and the χ^2_{red} of the fit. The energy value marked with an asterisk differs from the one in Table I, where it is 23 934.20(5) cm^{-1}, because the frequency was not adjusted to the centroid during scanning of the second laser. The only observed series converging directly to the IP is marked with a dagger. From the same level at 24 338.23 cm^{-1} both an s- and a d-series were observed converging to the first excited level in the ^{254}Es$^+$ ion. The final result is given in bold and the mean of the individual values with a statistical uncertainty given by the standard error of the mean.

E_1 (cm^{-1})	n	δ_0	δ_1	Convergence limit (cm^{-1})	IP (cm^{-1})	χ^2_{red}
23 933.40*	14-39	3.746(3)	–3.1(4)	52 303.86(11)	51 365.21(11)	0.6
24 338.23	20–31, 33–35, 40–43	3.678(4)		51 364.50(12)[a]	51 364.50(12)	0.6
24 338.23	14–40	3.710(2)		52 303.30(13)	51 364.65(13)	3.6
24 338.23	14, 16–25	5.435(2)		52 303.30(33)	51 364.65(33)	7.7
24 489.12	18–41	3.691(2)		52 303.53(10)	51 364.88(10)	0.4
25 433.26	14–29	3.763(16)	–5.3(17)	52 303.42(48)	51 364.77(48)	7.0
26 357.00	16–20, 23, 25–34	3.696(4)		52 302.70(29)	51 364.05(29)	4.6
28 118.49	17–19, 25–36	3.685(3)		52 302.52(24)	51 363.87(24)	1.7
28 578.49	16–31	3.773(11)	–6.8(16)	52 303.32(29)	51 364.67(29)	0.6
				Mean value	**51 364.58(14)**	

the isoelectronic homologue of einsteinium [35]. Finally, we can plot the energy of the Rydberg states in dependence of the principal quantum number as shown in Fig. 9. Fitting Eq. (1) to the data delivers a precise determination of the series limit. In a first analysis step, only the first term of the expansion in Eq. (2) was considered, and then the residuals were plotted. Hereby, some series showed a statistical distribution of the peaks, some a systematic trend. In the latter case, also the second term was used to improve the fit. Some of the series also seem to be disturbed by interlopers [36], as inferred from increased values of χ^2_{red} in Table III. However, an exact treatment of interlopers is most often ambiguous and their influence on the fit results is negligible. We only considered series with at least ten assigned resonances. Table III gives an overview of all identified series and the extracted series limits. The uncertainties for each series include both, the uncertainty of the FES and that of the fit. Note that the indirect IP determination via the series limit to the first excited state in Es II at 938.65 cm^{-1} is affected by the isotope shift, since this

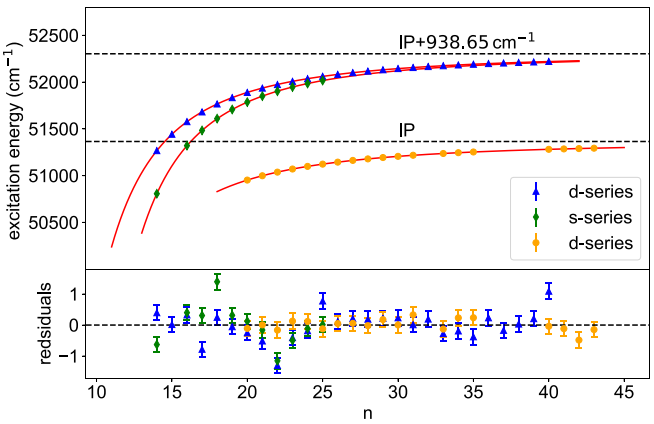

FIG. 9. Rydberg-Ritz fit to the s- and d-series extracted from Fig. 7 converging to the ionic ground state and the lowest-lying excited state in the Es$^+$ ion.

state is only measured for ^{253}Es [21] and all measurements here refer to ^{254}Es. However, we estimate this shift to be negligible compared to other uncertainties, considering an isotope shift of $\delta\nu^{253,254} = -0.17$ cm^{-1} in the $7s^2$ to $7s7p$ transition No. 9 [26]. The large hyperfine splitting in the energy levels in einsteinium limits our accuracy. For example, the ground state of ^{254}Es has a total splitting of 1.29 cm^{-1} [26]. Using the magnetic moment determined in [26] in combination with the hyperfine structure parameters in [21], one can calculate the total hyperfine splitting in the ^{254}Es$^+$ ion for the ground state and lowest excited state to 5.91 cm^{-1} and 2.96 cm^{-1}, respectively (see Fig. 11). This also explains the variations in the results for the different series, which do not overlap within their statistical uncertainties. For the level at 23 934.2 cm^{-1}, the excitation laser was detuned by approximately -0.8 cm^{-1} from the centroid, which leads to an increased population of specific hyperfine levels. In this case especially for relatively low-lying F levels around $F = 15/2$. This bias propagates to the total excitation energies of the Rydberg series and could explain the slightly higher value of the convergence limit for this series compared to all others. According to Fig. 11 lower final F values correspond to higher energies in the first excited state of the ion, while the order is reversed in the ground state. As we subtract the centroid of the state, this might lead to a systematic shift to a higher value of the IP. We determine the IP by averaging all convergence limits, taking the standard error of the mean as statistical uncertainty. A systematic deviation can occur due to the broad hyperfine structure in the ground state and the first excited state in the ^{254}Es$^+$ ion. For FES No. 2, we measured series converging to both, ionic ground and first excited state, resulting in a deviation of the determined IP of only 0.15 cm^{-1}. In these series, similar F values must be populated, since the first steps remained constant during the scan. However, the convergence limit can only match for similar F values if their values are near the center of both levels, as the order of their hyperfine levels opposite (see Fig. 11). A systematic uncertainty of 0.5 cm^{-1}, accounting for the fact that we can not exactly define the

prominent F value, thus represents a conservative setting of this uncertainty. Finally, we obtain an value of

$$E_{\mathrm{IP}} = 51\,364.58(14)_{\mathrm{stat}}(50)_{\mathrm{sys}}\ \mathrm{cm}^{-1}.$$

This is about 2.6σ above the current literature value of $E_{\mathrm{IP}} = 51\,358(5)\ \mathrm{cm}^{-1}$ (2σ uncertainty) [18,19]. We conclude that the uncertainty stated therein might be underestimated or a systematic effect might have been present which was not accounted for. The technique of field ionization was also applied for the determination of the IP for other actinides, e.g., californium [19]. For this element, we have since remeasured the IP, and similarly obtained higher values, supporting the assumption of a systematic effect [37]. The measurements presented here, in which many different series were measured and the results were averaged, reduce the uncertainties, which arise due to the hyperfine splitting of the first excited state in the ion.

IV. CONCLUSIONS

We collected a wide range of spectroscopic information on the atomic spectrum of einsteinium by resonance ionization laser spectroscopy using pg-sample amounts. Ten even-parity excited levels were identified by ground-state transitions, of which three were observed for the first time. Besides the level energies also the lifetimes of these states were determined. The search for AIS yielded efficient ionization schemes, which will enable future high-resolution measurements for investigating nuclear properties of more exotic and short-lived einsteinium isotopes, as well as sensitive ultratrace detection of einsteinium in specific radioactive samples stemming, e.g., from nuclear weapons fallout. We also identified 37 odd-parity energy levels for the first time. By combining these data with known spectral lines, energy level positions of some yet unobserved levels could be suggested (see Appendix B). The IP was determined by a detailed analysis of Rydberg series converging to the ground state and the first excited state in the Es^{+} ion, resulting in a value of $E_{\mathrm{IP}} = 51\,364.58(14)_{\mathrm{stat}}(50)_{\mathrm{sys}}\ \mathrm{cm}^{-1}$. This is about 2.6σ above the former literature value [18], but a factor of four more precise than this.

ACKNOWLEDGMENTS

This research was supported by the U.S. Department of Energy, Office of Science, Office of Basic Energy Sciences, Heavy Elements Chemistry Program, under Award No. DE-FG02-13ER16414. The isotope used in this research was supplied by the U.S. DOE Isotope Program, managed by the Office of Science. This work has been supported by the Bundesministerium für Bildung und Forschung (BMBF, Germany) under Grant No. 05P18UMCIA. This project has received funding from the European Union's Horizon 2020 research and innovation programme under Grant Agreement No. 861198-LISA-H2020-MSCA-ITN-2019.

APPENDIX A: FIRST EXCITATION STEP

In Fig. 10, the laser scans of the FES with higher resolution are shown in comparison to the data obtained from a broadband frequency scan. All FES are drawn relative to their centroid as given in Table I. More information about the high-resolution data can be found in [26]. The comparison between both methods allows to determine the uncertainty to 0.25 cm^{-1} for fast frequency scan with low resolution.

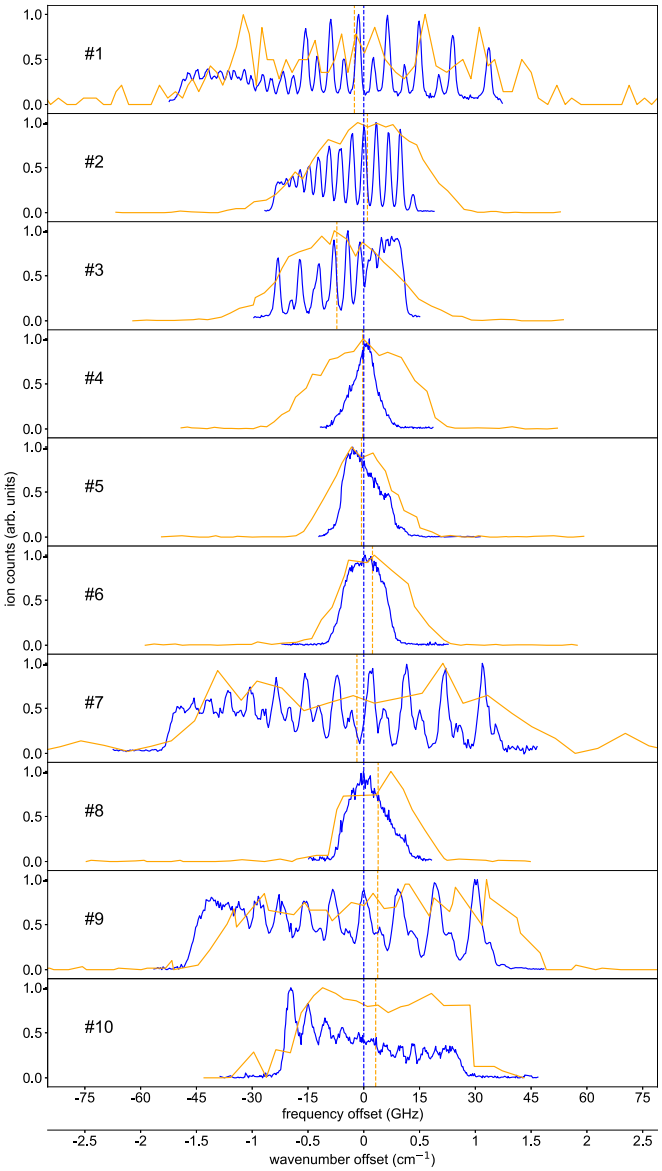

FIG. 10. Comparison of the frequency scans with higher resolution (blue) and the data obtained in the long-range scan (orange). All FES are drawn relative to their centroid (dashed-blue line) as given in Table I. The dashed-orange line indicates the centroid determined in the broadband laser scan by just applying a Gaussian fit, the deviation in all 10 cases is below 0.25 cm^{-1}.

APPENDIX B: SYSTEMATIC STUDIES OF THE SPECTRA

From the 290 spectral lines observed in 1974, only a few could be assigned to specific energy levels at that time. Wyart *et al.* pointed to the unexplored infrared region of the Es I spectrum as one of the reasons for the slow advances [15]. In Sec. III C, we presented the results from different laser scans in the near-infrared region and were able to newly

TABLE IV. Potential energy values for 31 even-parity levels as obtained by allocating a minimum of four so far unassigned transitions from [14] with energy levels from Table II. Existing states should be detectable within 0.5 cm^{-1} around the specified value.

Possible even-parity energy levels (cm^{-1})			
4523.1	4540.3	4887.0	5176.8
5301.6	9698.8	11 305.0	11 461.4
11 716.4	12 094.5	12 365.6	12 428.9
12 474.7	12 564.3	12 617.3	12 901.9
12 925.8	12 959.9	13 057.1	13 171.5
13 172.9	13 194.6	13 410.4	13 530.3
13 660.0	13 799.4	13 891.0	14 100.5
14 197.8	14 961.6	15 017.2	

assign 37 and confirm 11 previously allocated energy levels in this region. Comparing these energy levels with the list of unassigned spectral lines in [14] leads to a suggestion of unknown energy level positions. At first, all lines assigned to the Es II spectrum and known Es I transitions are excluded. Furthermore, lines, which are reported within 0.5 cm^{-1} are considered as a single line for analysis. From each of the high-lying level energies listed in Table II, the energies of the remaining 231 lines were subtracted. This generates a list of more than 11 000 possible energetic positions for even-parity states. In Table IV, we give 31 energy positions where at least four of these are located within 0.5 cm^{-1}. Of course, this is a rather vague requirement and some clusters are expected for purely statistical reasons. Nevertheless, the 23 levels between 11 000 cm^{-1} and 14 200 cm^{-1} are accessible with a fundamental Ti:sapphire laser and could be investigated regarding their existence in future measurements.

APPENDIX C: HYPERFINE SPLITTING IN THE $^{254}Es^{+}$ ION

To accurately determine the first ionization potential, it is necessary to look at the hyperfine structure splitting of the $^{254}Es^{+}$ ground state and first excited state. Taking the magnetic and quadrupole moment determined in Ref. [26] and the hyperfine parameters in [21] for the $^{253}Es^{+}$ ion, one can calculate the total hyperfine splitting in the $^{254}Es^{+}$ ion for the ground state and lowest excited state. This is depicted in Fig. 11.

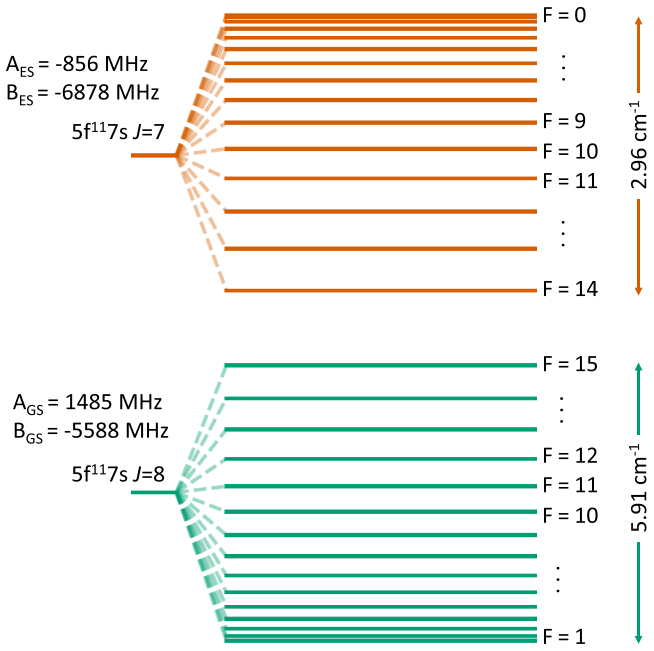

FIG. 11. Hyperfine structure splitting of the ground state (GS) and lowest-lying excited state (ES) in the $^{254}Es^{+}$ ion. The total splitting is given on the right.

[1] M. Block, M. Laatiaoui, and S. Raeder, Recent progress in laser spectroscopy of the actinides, Prog. Part. Nucl. Phys. **116**, 103834 (2021).

[2] D. E. Ferguson, ORNL transuranium program. The production of transuranium elements, Nucl. Sci. Eng. **17**, 435 (1963).

[3] M. Laatiaoui, W. Lauth, H. Backe, M. Block, D. Ackermann, B. Cheal, P. Chhetri, C. E. Düllmann, P. v. Duppen, J. Even *et al.*, Atom-at-a-time laser resonance ionization spectroscopy of nobelium, Nature (London) **538**, 495 (2016).

[4] P. Chhetri, D. Ackermann, H. Backe, M. Block, B. Cheal, C. Droese, C. E. Dullmann, J. Even, R. Ferrer, F. Giacoppo *et al.*, Precision Measurement of the First Ionization Potential of Nobelium, Phys. Rev. Lett. **120**, 263003 (2018).

[5] S. Raeder, D. Ackermann, H. Backe, R. Beerwerth, J. C. Berengut, M. Block, A. Borschevsky, B. Cheal, P. Chhetri, C. E. Dullmann *et al.*, Probing Sizes and Shapes of Nobelium Isotopes by Laser Spectroscopy, Phys. Rev. Lett. **120**, 232503 (2018).

[6] A. Ghiorso, S. G. Thompson, G. H. Higgins, G. T. Seaborg, M. H. Studier, P. R. Fields, S. M. Fried, H. Diamond, J. F. Mech, G. L. Pyle, J. R. Huizenga, A. Hirsch, W. M. Manning, C. I. Browne, H. L. Smith, and R. W. Spence, New elements einsteinium and fermium, atomic numbers 99 and 100, Phys. Rev. **99**, 1048 (1955).

[7] S. G. Thompson, A. Ghiorso, B. G. Harvey, and G. R. Choppin, Transcurium isotopes produced in the neutron irradiation of plutonium, Phys. Rev. **93**, 908 (1954).

[8] M. H. Studier, P. R. Fields, H. Diamond, J. F. Mech, A. M. Friedman, P. A. Sellers, G. Pyle, C. M. Stevens, L. B. Magnusson, and J. R. Huizenga, Elements 99 and 100 from pile-irradiated plutonium, Phys. Rev. **93**, 1428 (1954).

[9] P. R. Fields, M. H. Studier, J. F. Mech, H. Diamond, A. M. Friedman, L. B. Magnusson, and J. R. Huizenga, Additional properties of isotopes of elements 99 and 100, Phys. Rev. **94**, 209 (1954).

[10] G. R. Choppin, S. G. Thompson, A. Ghiorso, and B. G. Harvey, Nuclear properties of some isotopes of californium, elements 99 and 100, Phys. Rev. **94**, 1080 (1954).

[11] A. Ghiorso, G. B. Rossi, B. G. Harvey, and S. G. Thompson, Reactions of U^{238} with cyclotron-produced nitrogen ions, Phys. Rev. **93**, 257 (1954).

[12] E. F. Worden, R. G. Gutmacher, R. W. Lougheed, J. E. Evans, and J. G. Conway, Hyperfine structure in the ^{253}Es emission spectrum, J. Opt. Soc. Am. **58**, 998 (1968).

[13] E. F. Worden, R. G. Gutmacher, R. W. Lougheed, J. G. Conway, and R. J. Mehlhorn, Hyperfine structure in the ^{253}Es emission spectrum. II. Nuclear spin, nuclear magnetic dipole moment, and energy levels of Es ii, J. Opt. Soc. Am. **60**, 1297 (1970).

[14] E. F. Worden, R. W. Lougheed, R. G. Gutmacher, and J. G. Conway, Hyperfine structure in the ^{253}Es emission spectrum, III: Extension of the line list, levels of Es I and Es II, nuclear magnetic-dipole and quadrupole moments, J. Opt. Soc. Am. **64**, 77 (1974).

[15] J. F. Wyart, J. Blaise, and E. F. Worden, Studies of electronic configurations in the emission spectra of lanthanides and actinides: Application to the interpretation of Es I and Es II, predictions for Fm I, J. Solid State Chem. **178**, 589 (2005).

[16] G. S. Hurst, M. G. Payne, S. D. Kramer, and J. P. Young, Resonance ionization spectroscopy and one-atom detection, Rev. Mod. Phys. **51**, 767 (1979).

[17] V. S. Letokhov and V. I. Mishin, Highly selective multistep ionization of atoms by laser radiation, Opt. Commun. **29**, 168 (1979).

[18] J. R. Peterson, N. Erdmann, M. Nunnemann, K. Eberhardt, G. Huber, J. V. Kratz, G. Passler, O. Stetzer, P.Thörle, N. Trautmann, and A. Waldek, Determination of the first ionization potential of einsteinium by resonance ionization mass spectroscopy (RIMS), J. Alloys Compd. **271-273**, 876 (1998).

[19] N. Erdmann, M. Nunnemann, K. Eberhardt, G. Huber, S. Köhler, J. V. Kratz, G. Passler, J. R. Peterson, N. Trautmann, and A. Waldek, Determination of the first ionization potential of nine actinide elements by resonance ionization mass spectroscopy (RIMS), J. Alloys Compd. **271-273**, 837 (1998).

[20] D. Studer, S. Heinitz, R. Heinke, P. Naubereit, R. Dressler, C. Guerrero, U. Köster, D. Schumann, and K. Wendt, Atomic transitions and the first ionization potential of promethium determined by laser spectroscopy, Phys. Rev. A **99**, 062513 (2019).

[21] J. Blaise and J. F. Wyart, Selected constants energy levels and atomic spectra of actinides, *Centre National de la Recherche Scientifique (CNRS) (1992)*, https://inis.iaea.org/search/search-singlerecord.aspx?recordsFor=SingleRecord&RN=24031406.

[22] L. S. Goodman, H. Diamond, and H. E. Stanton, Nuclear and atomic moments and hyperfine-structure parameters of ^{253}Es and ^{254m}Es, Phys. Rev. A **11**, 499 (1975).

[23] V. N. Fedosseev, L.-E. Berg, N. Lebas, O. J. Launila, M. Lindroos, R. Losito, B. A. Marsh, F. K. Österdahl, T. Pauchard, G. Tranströmer, and J. Vannesjö, ISOLDE RILIS: New beams, new facilities, Nucl. Instrum. Methods Phys. Res., Sect. B **266**, 4378 (2008).

[24] T. Kieck, S. Biebricher, Ch. E. Düllmann, and K. Wendt, Optimization of a laser ion source for ^{163}Ho isotope separation, Rev. Sci. Instrum. **90**, 053304 (2019).

[25] K. Zhang, D. Studer, F. Weber, V. M. Gadelshin, N. Kneip, S. Raeder, D. Budker, K. Wendt, T. Kieck, S. G. Porsev, C. Cheung, M. S. Safronova, and M. G. Kozlov, Detection of the Lowest-Lying Odd-Parity Atomic Levels in Actinium, Phys. Rev. Lett. **125**, 073001 (2020).

[26] S. Nothhelfer, T. E. Albrecht-Schonzart, M. Block, P. Chhetri, C. E. Dullmann, J. G. Ezold, V. Gadelshin, A. Gaiser, F. Giacoppo, R. Heinke *et al.*, Nuclear structure investigations of $^{253-255}$Es by laser spectroscopy, Phys. Rev. C **105**, L021302 (2022).

[27] J. B. Roberto, C. W. Alexander, R. A. Boll, J. D. Burns, J. G. Ezold, L. K. Felker, S. L. Hogle, and K. P. Rykaczewski, Actinide targets for the synthesis of super-heavy elements, Nucl. Phys. A **944**, 99 (2015).

[28] S. Rothe, B. A. Marsh, C. Mattolat, V. N. Fedosseev, and K. Wendt, A complementary laser system for ISOLDE RILIS, J. Phys.: Conf. Ser. **312**, 052020 (2011).

[29] M. Raiwa, S. Büchner, N. Kneip, M. Weiß, P. Hanemann, P. Fraatz *et al.*, Actinide imaging in environmental hot particles from Chernobyl by rapid spatially resolved resonant laser secondary neutral mass spectrometry, Spectrochimica Acta Part B: Atomic Spectroscopy **190**, 106377 (2022).

[30] G. C. King, F. H. Read, and R. E. Imhof, The measurement of molecular lifetimes by the photon-photon delayed coincidence method, J. Phys. B: At. Mol. Phys. **8**, 665 (1975).

[31] D. Studer, L. Maske, P. Windpassinger, and K. Wendt, Laser spectroscopy of the 1001-nm ground-state transition in dysprosium, Phys. Rev. A **98**, 042504 (2018).

[32] R. P. de Groote, M. Verlinde, V. Sonnenschein, K. T. Flanagan, I. Moore, and G. Neyens, Efficient, high-resolution resonance laser ionization spectroscopy using weak transitions to long-lived excited states, Phys. Rev. A **95**, 032502 (2017).

[33] W. Ritz, Zur Theorie der Serienspektren, Ann. Phys. (Paris) **317**, 264 (1903).

[34] U. Fano, C. E. Theodosiou, and J. L. Dehmer, Electron-optical properties of atomic fields, Rev. Mod. Phys. **48**, 49 (1976).

[35] J. Hostetter, J. D. Pritchard, J. E. Lawler, and M. Saffman, Measurement of holmium Rydberg series through magneto-optical trap depletion spectroscopy, Phys. Rev. A **91**, 012507 (2015).

[36] M. J. Seaton, Quantum defect theory, Rep. Prog. Phys. **46**, 167 (1983).

[37] F. Weber, Ch. E. Düllmann, V. Gadelshin, N. Kneip, S. Oberstedt, S. Raeder, J. Runke, C. Mokry, P. Thörle-Pospiech, D. Studer, N. Trautmann, and K. Wendt, Probing the atomic structure of californium by resonance ionization spectroscopy, Atoms **10**, 51 (2022).